Soft Matter

Soft Matter from Liquid Crystals

Journal:	*Soft Matter*
Manuscript ID	SM-PER-07-2019-001424.R1
Article Type:	Perspective
Date Submitted by the Author:	10-Aug-2019
Complete List of Authors:	Abbott, Nicholas; Cornell University, Department of Chemical and Biomolecular Engineering Kim, Youngki; POSTECH, Chemical Engineering Noh, JungHyun; Cornell University, Department of Chemical and Biomolecular Engineering Nayani, Karthik; Cornell University, Department of Chemical and Biomolecular Engineering

Soft Matter from Liquid Crystals

Young-Ki Kim,[a,b] JungHyun Noh,[a] Karthik Nayani,[a] and Nicholas L. Abbott*[a]

[a] Smith School of Chemical and Biomolecular Engineering, Cornell University, 113 Ho Plaza, Ithaca, New York 14853, United States

[b] Department of Chemical Engineering, Pohang University of Science and Technology, 77 Cheongam-Ro, Nam-Gu, Pohang, Gyengbuk 37673, Korea

Abstract

Liquid crystals (LCs) are fluids within which molecules exhibit long-range orientational order, leading to anisotropic properties such as optical birefringence and curvature elasticity. Because the ordering of molecules within LCs can be altered by weak external stimuli, LCs have been widely used to create soft matter systems that respond optically to electric fields (LC display), temperature (LC thermometer) or molecular adsorbates (LC chemical sensor). More recent studies, however, have moved beyond investigations of optical responses of LCs to explore the design of complex LC-based soft matter systems that offer the potential to realize more sophisticated functions (e.g., autonomous, self-regulating chemical responses to mechanical stimuli) by directing the interactions of small molecules, synthetic colloids and living cells dispersed within the bulk of LCs or at their interfaces. These studies are also increasingly focusing on LC systems driven beyond equilibrium states. This review presents one perspective on these advances, with an emphasis on the discovery of fundamental phenomena that may enable new technologies. Three areas of progress are highlighted; i) directed assembly of amphiphilic molecules either within topological defects of LCs or at aqueous interfaces of LCs, ii) templated polymerization in LCs via chemical vapor deposition, an approach that overcomes fundamental challenges related to control of LC phase behavior during polymerization, and iii) studies of colloids in LCs, including chiral colloids, soft colloids that are strained by LCs, and active colloids that are driven into organized states by dissipation of energy (e.g. bacteria). These examples, and key unresolved issues discussed at the end of this perspective, serve to convey the message that soft matter systems that integrate ideas from LC, surfactant, polymer and colloid sciences define fertile territory for fundamental studies and creation of future transformative technologies.

1. Introduction

The discovery and history of liquid crystals (LCs), which starts in 1888, illustrates the opportunity that emerges from research that crosses disciplinary boundaries: chemist-botanist Friedrich Reinitzer in Prague noticed that benzoic acid derivatives of cholesterol exhibited two melting points; he contacted physicist Otto Lehmann in Aachen, who identified the intermediate phase, the LC phase, to possess the mobility of isotropic liquids and long-range ordering of crystalline solids.[1, 2] As a second example, research on LCs in the second half of the twentieth century was largely driven by the broad goal of elucidating the electro-optical properties of LCs, a challenge that required the cross-disciplinary collaboration of chemists to create chemically stable LCs, and physicists and electrical engineers to understand the response of LCs to external fields under confinement.[3-5] In the past two decades, research involving LCs has continued to show the value of transdisciplinary efforts, with a particular focus on exploration of intellectual intersections between LC science and other fields of soft matter research involving surfactants (self-assembly at aqueous-LC interfaces[6-9] including biological lipids[8-15]), polymers (polymerization in LC defects of blue phases[16-20]) and colloids (assembly directed by LCs[21-27], including formation of organized arrays[24-29]). In this Perspective Article, we do not comprehensively review all recent efforts at the interface between *LC science* and *surfactant*, *polymer* and *colloid sciences* but instead we focus on several specific advances that illustrate these themes.

The first section, which involves LCs and *surfactant science*, describes the use of topological defects in LCs to selectively trigger the self-assembly of amphiphiles under conditions wherein the amphiphiles are singly dispersed in the bulk of the LC (Section 2.1). By cross-linking amphiphilic assemblies formed in defects and characterizing the resulting nanostructures by electron microscopy, new knowledge regarding the structure of defect cores on sub-optical scales has been obtained.[30] We also describe a series of studies that have advanced our understanding of the orientations of LCs at amphiphile-laden aqueous-LC interfaces (Section 2.2). Recent measurements[31, 32] have led to the understanding that amphiphiles at the LC interface can influence LC orientations through mechanisms of interaction that are strikingly different from the classical view of interdigitation of LC molecules with aliphatic tails of amphiphiles.[33, 34] These new studies suggest that some amphiphiles influence LC orientations via induction of local disorder in the LC near the amphiphile-decorated interface.[31, 32] This understanding has guided the design of

ultrasensitive LC sensors that respond to targeted chemical and biological species,[35, 36] and synthetic molecules that trigger multiscale responses in LCs.[37, 38]

In the second section of this Perspective Article, we explore the intersection of *polymer science* and recent LC research (Section 3), highlighting a new method for the synthesis of polymeric micro- and nanoparticles templated from either LC droplets with distinct internal configurations[39, 40] or topological defects[30, 41] (Section 3.1). Additionally, we describe a recent study that has established a new method for LC-templated synthesis of polymeric structures based on chemical vapor deposition (Section 3.2).[42] By continuously partitioning monomers into the LC from the vapor phase during polymerization, the method minimizes monomer-induced changes to LC phase behavior and enables synthesis of polymeric structures with programmable shape, size, lateral organization, and functionalities (e.g., adhesion, wetting, conductivity).

The last section (Section 4) of this Perspective Article addresses recent advances in research related to *colloids* in LCs. Following a brief overview of early seminal studies of spherical colloids in LCs, we describe recent studies of non-spherical particles in LCs that have identified colloid shape, including the number of sides and chirality of colloids, to be key factors that influences interparticle interactions in LCs (Section 4.1).[43-46] We also summarize recent studies of soft biological colloids in LCs (e.g., phospholipid vesicles), where elastic stresses generated by strained states of LCs have been shown experimentally and theoretically to drive dynamic transitions in the shapes and properties of soft colloids (Section 4.2).[47, 48] Finally, we comment on recent studies that have explored LC systems that are driven beyond equilibrium. Among these studies, we focus on several recent advances involving self-propelled colloids at LC interfaces (Section 4.3)[49] and motions of bacteria that are coupled to LC ordering (Section 4.4 and 4.5)[50, 51].

2. LCs and Surfactant Science

2.1. Molecular Self-Assembly in Topological Defects

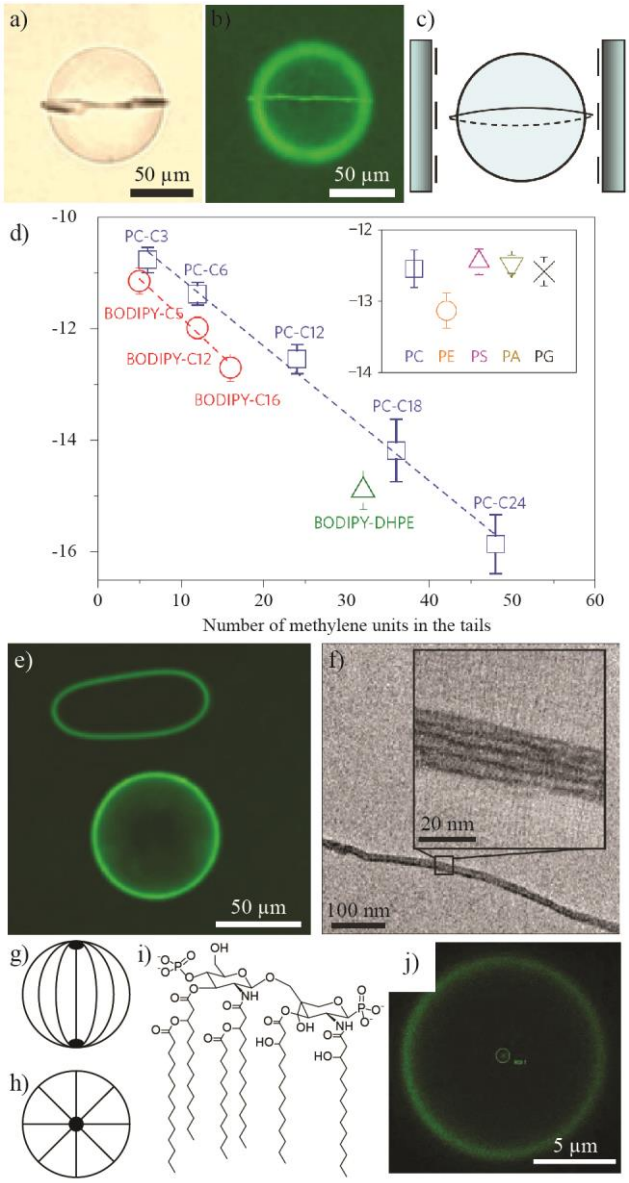

Fig. 1 **(a)** Bright field and **(b)** fluorescence micrographs showing the selective assembly of amphiphilic molecules within a 'Saturn-ring' defect (disclination loop of strength $m = -1/2$) formed around a microparticle dispersed in nematic LC. **(c)** Schematic illustration of the Saturn-ring. **(d)** Standard free energy (ΔG_1^0) of transfer of a BODIPY-labelled amphiphile or phospholipid (BODIPY-C*n* or PC-C*n* where *n* indicates the number of methylene units in each tail) from bulk LC to the disclination of strength $m = -1/2$. PC, phosphatidylcholine; PE, phosphatidylethanolamine; PS, phosphatidylserine; PA, phosphatidic acid; PG, phosphatidylglycerol. **(e)** Fluorescence micrograph of the polymerized 'O-ring' of amphiphiles that was displaced from the equator of the microparticle upon heating the nematic LC into an

isotropic phase. **(f)** TEM image of the polymerized structure of **e**, exhibiting a lamellar structure. **(g, h)** Schematic illustrations of LC ordering (solid lines) and topological defects (black dots) in LC droplets with **(g)** bipolar and **(h)** radial configurations. **(i)** Molecular structure of the bacterial lipid A (endotoxin). **(j)** Confocal fluorescence micrograph showing the localization of the fluorescently labelled lipid A at the topological defect, at the center of a LC droplet, in the radial configuration. Images are adapted with permissions from refs. 35 and 41.

As noted above, past studies have reported that topological defects formed within LCs can guide the assembly of polymers, and nano- and micro-particles. [16-27, 52-57] In this section, we move beyond this past focus by describing recent investigations of the directed assembly of small molecules within defects. We use the term "small" to refer to molecules or building blocks that are smaller than the size of the core region of a singular defect, the latter which depends strongly on the type of LC. For example, for a thermotropic LC, the diameter of the core of a defect is typically about 10 nm [1, 2, 52] whereas it can grow to as large as a few micrometers in lyotropic LCs.[58] In general, the cores of singular defects in LCs are characterized by a level of local orientational order that is low compared to the bulk LC (and in some cases, differing also in symmetry; e.g., uniaxial bulk order and biaxial order in defect[2, 58-60]). The local disordering represents a mechanism by which the elastic free energy density of the LC is bounded – in the absence of disorder, the elastic free energy would diverge at a singular defect. The strain-induced disordering of molecules within a defect core leads to a free energy density that is substantially higher than bulk LC, and thus defect cores tend to attract nanoscopic inclusions present within LCs.[1, 2, 52]

Recent advances in this area of research include the observation that non-mesogenic molecules preferentially partition towards defect cores in mixtures of mesogenic and non-mesogenic species. Soule *et al*.[61] theoretically predicted that the equilibrium concentration of non-mesogenic molecules is higher in the core of a point defect of strength +1 than in the bulk LC. We note that the strength of a 2D topological defect is defined as $m = \pm \alpha / 2\pi$, where α is the angle of rotation of the LC director **n** during a circumnavigation of the defect core (the sign of m is positive when the traveling and rotation directions are the same)[2]. 3D point defects can also be described by a charge N indicating how many times one meets all possible orientations of the vector field while moving around a closed surface surrounding the defect; $N = \frac{1}{4\pi} \oiint \mathbf{n} \left(\frac{\partial \mathbf{n}}{\partial u} \times \frac{\partial \mathbf{n}}{\partial v} \right) dudv$, where

u and *v* are arbitrary coordinates on the closed surface[58, 62, 63]. Subsequently, Wang *et al.*[41] experimentally demonstrated that small amphiphilic molecules partition into the nanoscopic cores of line defects (disclination) of $m = \pm 1/2$ in thermotropic LCs, and self-assemble into organized nanostructures. The work was motivated by an analogy to self-assembly of amphiphilic molecules in aqueous systems containing hydrophobic polymers (the defects playing the role of virtual polymers), although, as discussed below, important differences exist between the driving force for self-assembly in structured solvents such as water and nematic LCs.

Self-assembly of the amphiphiles within LC defects was characterized by several experimental approaches.[41] First, partitioning of amphiphiles into defects was imaged by using amphiphiles labeled with dipyrromethene boron difluoride (BODIPY), a fluorophore that exhibits a dimer emission upon self-association. These measurements revealed a critical aggregation concentration (CAC) above which fatty acids assembled within a disclination loop of $m = -1/2$ (so-called "Saturn ring" defect, Fig. 1a-c) formed around a microsphere dispersed in LC (homeotropic surface anchoring). Interestingly, in contrast to the predictions of Rey *et al*,[61] the BODIPY fluorophore, alone, did not partition preferentially from the bulk LC into the defect. Additionally, self-assembly of the amphiphiles containing BODIPY was not observed in the bulk of the LC (only in the defects). The CAC values measured in the defects were used to calculate a standard free energy of transfer (ΔG_1^0) of a homologous series of amphiphiles from bulk LC to assemblies formed within the cores of the $m = -1/2$ defects. ΔG_1^0 was found to be linearly dependent on the tail length of the amphiphiles (Fig. 1d). This result implies that the driving force for self-assembly of amphiphiles in defect cores is influenced by the length of the tail, similar to the effect of amphiphile tail length observed with self-assembly in water. The magnitude, however, is different; 0.13 K_BT per methylene in LC and ~0.69 K_BT per methylene for aqueous solutions, where K_B is the Boltzmann constant and T is the temperature.

Additional evidence of formation of organized amphiphilic assemblies within defects cores was obtained by using cryogenic transmission electron microscopy (cryo-TEM).[41] Examinations of blue phase LCs, which have a high density of $m = -1/2$ disclinations, revealed formation of organized assemblies of the phospholipid 1,2-dilauroyl-sn-glycero-3-phosphocholine (PC-C12) within the network of disclinations. The mean diameters of the assembles was measured to be 28 ± 4 nm, corresponding to ~9 lipid bilayers. In addition, a photoreactive lipid containing diacetylenic tails (1,2-bis(10,12-tricosadiynoyl)-sn-glycero-3-phosphoethanolamine (diyne PC))

was also found to form assemblies within 'Saturn-ring' defect formed around microspheres in nematic LCs (Fig. 1a-c and e). In contrast to the assembly of PC-C12 formed in the disclination of the blue phase LC, TEM of the photo-crosslinked assembly of diyne PC showed a well-defined multi-lamellar nanostructure with 5 lipid bilayers (Fig. 1f).

An additional important consequence of molecular self-assembly in defects is that ΔG_1^0 is sufficiently large in some systems to trigger reconfiguration of LCs on optical scales. Specifically, micrometer-sized nematic LC droplets dispersed in an aqueous phase have been observed to undergo transitions from bipolar (Fig. 1g) to radial (Fig. 1h) configurations upon addition of bacterial glycophospholipid (endotoxin, Fig. 1i) to the aqueous phase.[35, 36, 64] The use of endotoxin labeled with a fluorophore confirmed localization of endotoxin at the central defect of the radial configuration (Fig. 1j). The transition occurs at endotoxin concentrations of ~1 pg/ml, a concentration that is six orders of magnitude lower than that at which lipids such as 1,2-dilauroyl-snglycero-3-phosphatidylcholine (DLPC) and 1,2-dioleoyl-sn-glycero-3-phosphatidylcholine (DOPC) trigger changes in the configuration of LC droplets.[65, 66] In contrast to DLPC and DOPC (each possessing two non-polar tails), the lipid A portion of endotoxin possesses six amphiphilic tails (Fig. 1i), thus providing a large hydrophobic driving force for partitioning from the aqueous phase into the LC droplets. Additionally, the molecular architecture of lipid A, which leads to inverse lyotropic phases,[64] is likely to be an additional important factor promoting self-assembly of endotoxin at the N = +1 defect at the center of the radial droplet (Fig. 1j). Support for the proposal that both the hydrophobicity and molecular architecture of lipid A of endotoxin play a key role in triggering configurational changes of LC droplets was obtained by performing a structure-property study in which a family of amphiphiles was synthesized to mimic key physicochemical properties of bacterial endotoxin (surface pressure−area isotherms; nanostructure formed within concentrated phases).[64] We also note that the response of LC droplets to endotoxin is influenced by the anchoring energy of the LC at the aqueous interface and the size of the LC droplets, the latter being significant in part because the saddle-splay elastic constant plays a central role in modulating the elastic energy of the LC droplets during configurational transitions.[36]

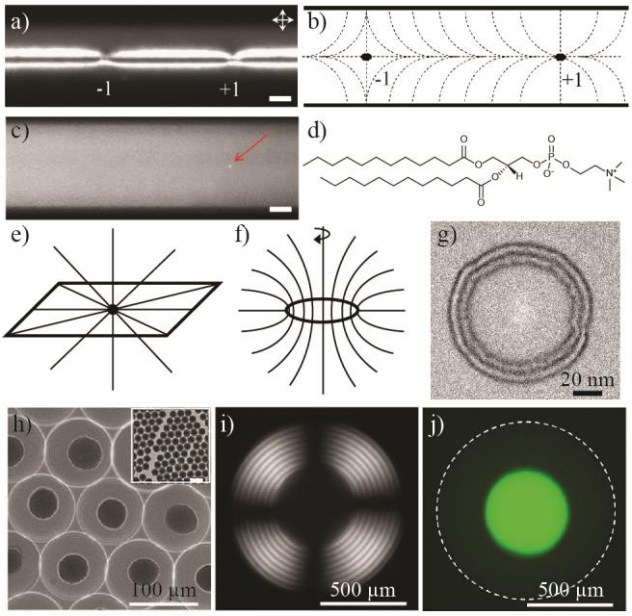

Fig. 2 **(a)** Optical micrograph (crossed polars) and **(b)** corresponding director profile of a pair of point defects with strength $N = \pm 1$, generated by confining a nematic LC within a capillary with a circular cross-section. **(c)** Fluorescence micrograph showing the selective assembly of phospholipids at the defect of strength $N = +1$. Scale bar, 100 µm. **(d)** Molecular structure of phospholipid DLPC. **(e, f)** Possible LC director profiles (solid lines) near **(e)** a point defect of strength $N = +1$ and **(f)** a disclination loop of strength $m = +1/2$. **(g)** TEM image of a molecular assembly of phospholipid templated by a defect that optically appears to be a point with strength $N = +1$. **(h)** Bright field, **(i)** polarizing, and **(j)** fluorescent micrographs of cholesteric lyotropic LC droplets containing fluorescent labelled nanoparticles with diameters of 184 nm. Images are adapted with permissions from refs. 30 and 68.

Recent studies have also shown that molecular self-assembly can be used to provide new physical insights into the nanostructure (structure below what can be resolved by far-field optical methods) of LC defect cores.[30] For example, an interesting series of conclusions have emerged from studies of molecular assembly of the phospholipid DLPC within the cores of point defects with $N = \pm 1$ (Fig. 2a-d).[30] Specifically, self-assembly of DLPC was observed within the core of defects with strength $N = +1$ (CAC $\approx$ 47 µM) but not with strength $N = -1$ (CAC $\approx$ 570 µM), as shown in Fig. 2c. This observation suggests that local ordering of the mesogens at or near a defect core influences whether or not molecular self-assembly of amphiphiles occurs within a defect. A full understanding of the influence of the strength of defects on molecular self-assembly, however,

is yet to be fully established. Second, lipid assemblies templated by point defects with $N = +1$ (Fig. 2e) were found to have a toroidal morphology suggesting that, at least in the presence of lipids, the +1 point defect (as characterized optically, Fig. 2a, e) is, in fact, a nanoscopic disclination loop of $m = +1/2$ (Fig. 2f, g). Finally, we comment that an additional recent study of molecular segregation in defects has addressed mixtures of mesogens. Atomistic simulations[67] were used to reveal that defects and interfaces can induce compositional segregation in LC mixtures. Specifically, simulations performed with mixtures of 5CB and 8CB predict that 5CB partitions preferentially into a defect core while 8CB molecules partition preferentially towards air interfaces (the enrichment of 8CB at interfaces yielded smectic layers, which excluded 5CB molecules). This study is broadly interesting because most technologically relevant LCs are mixtures. The results hint that a detailed understanding of the nanoscopic properties of LC mixtures may require a more complete consideration of local segregation of species within defects and at interfaces.

Whereas the discussion above is largely focused on molecular self-assembly in defects of thermotropic LCs, a number of interesting observations of defect-mediated self-assembly of colloids have been reported in lyotropic LC systems.[68] As noted above, in lyotropic systems, the sizes of defect cores can extend into the micrometer range,[58] thus enabling self-assembly of nanoparticles. For example, Kumacheva *et al.*[68] reported spontaneous accumulation of nanoparticles within micrometer-sized defect cores (6 − 17 μm in diameter) formed at the center of droplets of lyotropic cholesteric LCs prepared from cellulose nanocrystals (Fig. 2h-j). The segregation of nanoparticles to defect cores was found to be dependent on nanoparticle size, with nanoparticles with diameters of 184 nm localizing within the defect core but nanoparticles smaller than 54 nm not segregating to the core. Moreover, the study showed that the size of the defect core can be tuned by volume fraction of nanoparticles, expanding from a diameter of 6 − 17 μm in the absence of nanoparticles to a diameter of 50 μm in the presence of nanoparticles.[68]

2.2. Surfactants at Aqueous-LC Interfaces

The previous section of this Perspective Article describes the recent discovery that amphiphilic molecules can self-assemble in the defect cores of nematic LCs. While the discovery that organized molecular assemblies form within defects is recent, a large number of prior studies have established that amphiphilic molecules spontaneously assemble at LC interfaces to influence the

orientation of LCs.[6-10] Among the various LC interfaces studied (e.g., aqueous−LC, solid−LC, and air−LC interfaces), aqueous−LC interfaces are particularly interesting in the context of the design of stimuli-responsive LC materials because they permit facile delivery of adsorbates from an aqueous phase to the LC interface (enabling studies of biomolecular systems),[6, 8] can be created in a range of geometries (e.g., LC-in-water emulsions, allowing exploration of an interplay of surface anchoring, elastic, and defect energies in the response of LCs to molecular triggers),[35, 36] and provide adsorbates with high lateral mobility[65] (permitting rapid reorganization and spatial patterning of assemblies and LC in response to stimuli).

To provide insights into how amphiphiles impact the ordering of LCs at aqueous interfaces, two experimental set-ups have been used. As illustrated in Fig. 3a, one approach has employed micrometer-thick films of LC hosted in metallic grids (typically used for transmission electron microscopy (TEM)) supported on a treated glass substrate to impose homeotropic anchoring of the LC. As LCs typically assume a tangential orientation at aqueous interfaces in the absence of adsorbates, immersion of the LC film into an aqueous solution gives rise to hybrid anchoring conditions (Fig. 3a) that are signaled by a bright optical appearance (Fig. 3b).[31, 38] Alternatively, LC droplets have been used to explore the behavior of adsorbates at aqueous−LC interfaces as the internal configurations of LC microdroplets are strongly influenced by adsorbates (Fig. 1g, h). Rapid analysis of large populations of LC droplets has been performed by measuring light scattered by the droplets using a flow cytometry.[7, 38, 69]

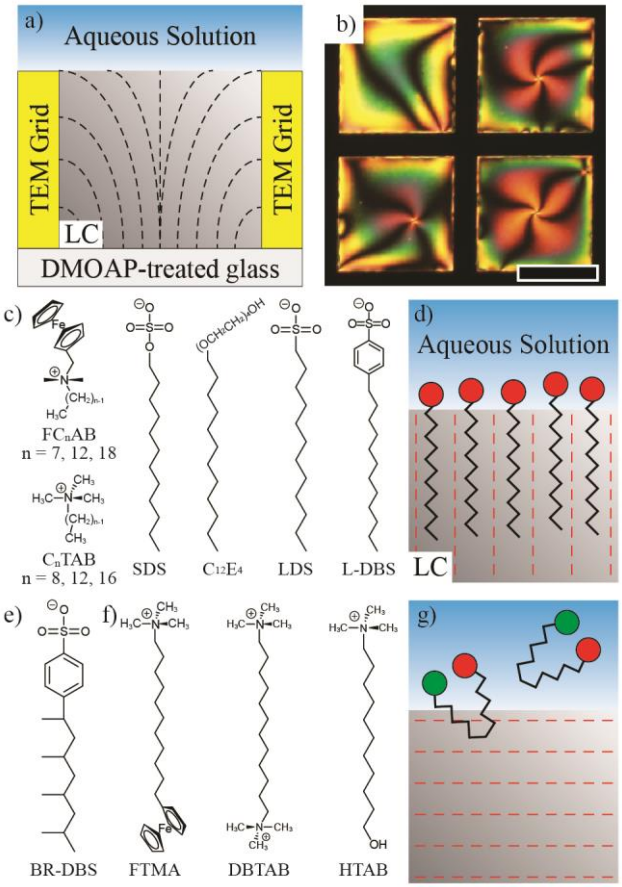

Fig. 3 **(a)** Schematic illustration (side view) and **(b)** optical micrograph (crossed polars, top view) of LC films hosted in a TEM grid (20 μm in thickness) supported on a DMOAP-treated glass substrate and immersed under an aqueous solution. Dashed lines in **a** indicate the LC director **n**. Scale bar in b, 200 μm. **(c)** Molecular structures of surfactants with linear tails: *N*,*N*-dimethylferrocenylalkylammonium bromides (FC_nAB); alkyltrimethylammonium halides (C_nTAB); Sodium dodecyl sulfate (SDS); monododecyl ether ($C_{12}E_4$); linear dodecanesulfonate (LDS), linear dodecylbenzenesulfonate (L-DBS). **(d)** Schematic illustration of the homeotropic orientation of LCs induced by linear surfactants in **c** at the aqueous−LC interface. **(e, f)** Molecular structures of surfactants with **(e)** branched tails and **(f)** "bolaform" architecture: branched dodecylbenzenesulfonate (BR-DBS); 11-(ferrocenylundecyl)trimethylammonium bromide (FTMA); dodecyl-1,12-bis(trimethylammonium bromide) (DBTAB); (11-hydroxyundecyl)trimethylammonium bromide (HTAB). **(g)** Schematic illustration showing that bolaform surfactants, when adsorbed at LC interfaces, do not cause homeotropic orientation of the LC. Images are adapted with permissions from refs. 33, 34, and 38.

By using the two experimental set-ups described above, Brake *et al* and Lockwood *et al.*[33, 34] provided experimental insight into mechanisms of interaction of amphiphiles and LCs at aqueous interfaces by examining families of surfactants with distinct molecular architectures. The studies revealed that classical surfactants with a single hydrophilic head and a single, linear hydrophobic tail (Fig. 3c) cause homeotropic LC orientations at aqueous−LC interfaces (Fig. 3d).[33] In contrast, surfactants with branched tails (Fig. 3e) or bolaform surfactants (Fig. 3f), which have two head groups and adopt looped conformations at the aqueous-LC interface, do not reorient LCs away from their initial tangential orientation in water (Fig. 3g).[33, 34] The influence of linear surfactants on LC anchoring was also found to be dependent on aliphatic tail length and the interfacial density of molecules. For example, only FC_nAB with $n > 8$ and C_nTAB with $n > 12$ (Fig. 3c) caused homeotropic anchoring of LCs at aqueous−LC interfaces at the highest densities of adsorbed surfactants. In addition, by comparing anchoring transitions caused by DTAB, SDS, and $C_{12}E_4$, each of which have same tail length but differ in headgroup, no measurable effect of head group type on the LC ordering was found.[33, 34] Overall, and most importantly, the results above are consistent with previously proposed mechanisms of interaction between the LC and surfactant that involves interdigitation of mesogens with the linear non-polar tails of amphiphilic molecules to generate the homeotropic orientation.[70-78] The experimental results are also consistent with the surfactants causing the easy axis of the LC (lowest free energy orientation) to transition to the perpendicular, a point that we return to below. Support for this interpretation of the mechanism by which surfactants influence LC anchoring at aqueous interfaces can be found in a literature addressing LC orientations at surfactant-decorated solid surfaces.[70-74]

In light of the above structure-property relationships that support the conclusion that interdigitation of the tails of amphiphiles into LCs leads to homeotropic LC orientations, a noteworthy recent development is the proposal that some amphiphiles, which also cause homeotropic orientations, trigger this orientation of the LC through a mechanism that is not dominated by interdigitation. Specifically, the alternative mechanism suggests that the homeotropic orientation can be observed without reorientation of easy axis but instead via lowering of the surface anchoring energy of the LCs such that elastic strain present in the initial hybrid anchoring of LC films (Fig. 3a) is relieved via adoption of the homeotropic orientation at the aqueous−LC interface.[31, 32] Experimental observations and molecular simulations support the proposal that the synthetic amphiphilic oligomer (AMP2, Fig. 4a) triggers homeotropic

orientations via this mechanism: upon adsorption of AMP2 at the aqueous interface of nematic 5CB, a LC film with hybrid anchoring (birefringent optical texture; Fig. 4b) was transformed into the homeotropic configuration (dark appearance; Fig. 4c). In contrast, a LC film supported on a solid surface with planar anchoring did not display an optical response to adsorption of AMP2, consistent with an anchoring transition in the hybrid film not caused by a change in easy axis but rather a change in anchoring energy (Fig. 4d, e). To provide additional insight into these observations, atomistic molecular dynamics simulations were carried out at aqueous-LC interfaces decorated with AMP2 (Fig. 4f, g). A key result of the simulations was that the nematic director is not well-defined within a region approximately 2 nm from the aqueous interface (green region in Fig. 4f). In this region, the scalar order parameter S is low ($S < 0.2$), suggesting a localized melting/disordering of the nematic phase induced by the amphiphile, whereas the average value of S remains ~0.55 in the bulk LC film. Overall, these results reveal that the impact of amphiphiles on local LC ordering near an interface, and thus the far-field LC orientation, is strongly influenced by the molecular structure of the amphiphiles in ways that have not yet been distilled into simple design rules.

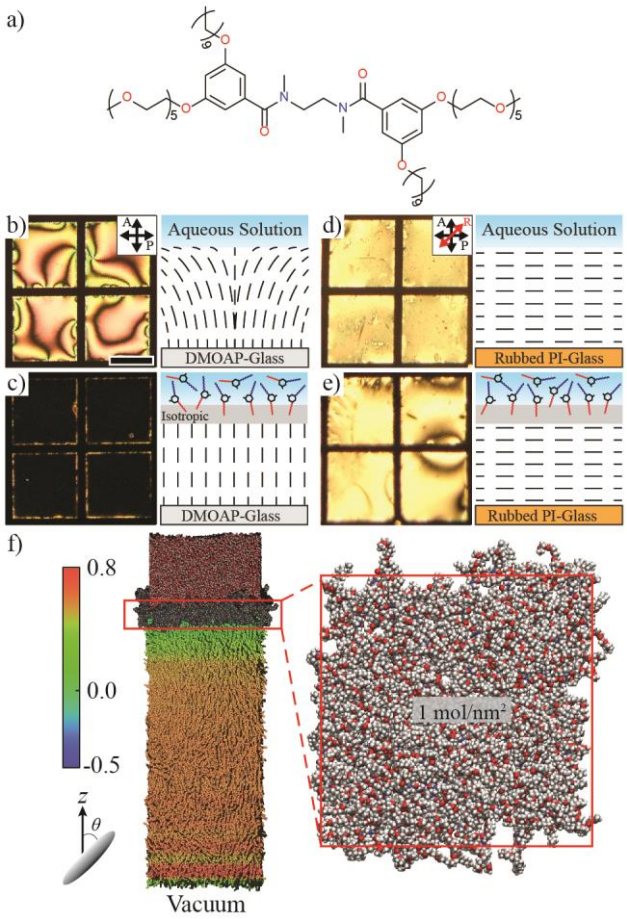

Fig. 4 **(a)** Molecular structure of amphiphilic oligomer, AMP2. **(b-e)** Optical micrographs (top view, crossed polars) and corresponding director profile (side view) of LC films (10 μm in thickness) supported on glass substrates coated with **(b, c)** DMOAP and **(d, e)** a rubbed polyamide following contact with aqueous solutions **(b, d)** without and **(c, e)** with 0.15 mM AMP2. "R", "P", and "A" indicate the rubbing direction and polarizations of polarizer and analyzer, respectively. Dashed lines in the second and fourth columns indicate **n**. Scale bar, 200 μm. **(f)** Molecular dynamics simulations of a LC film confined between vacuum and aqueous solution with AMP2. The color-coded profile indicates the scalar order parameter *S*. **(g)** Top-view snapshot of an AMP2 monolayer at the aqueous−LC interface in **f**. The monolayer of AMP2 was created by adding 1 mol/nm^2 of the amphiphiles to the aqueous−LC interface. Images are adapted with permissions from refs. 31 and 32.

3. LCs and Polymer Science

3.1. Templated Polymerization

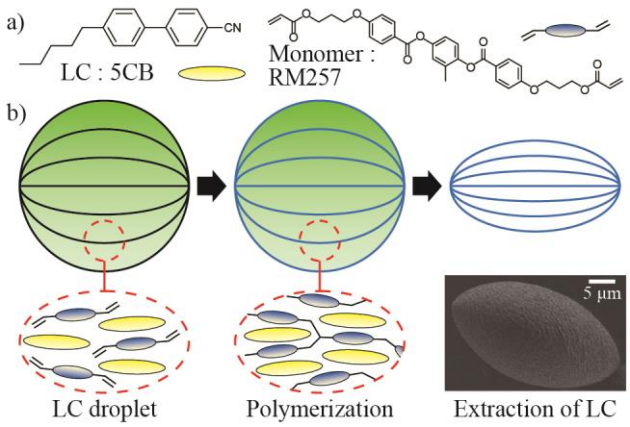

Fig. 5 (a) Molecular structures of 5CB and reactive mesogen RM257. **(b)** Schematic illustration of the synthesis of polymeric microparticles templated from LC droplets. Solid lines represent the orientation of 5CB and RM257. The final spindle-shaped microparticle is obtained following the extraction of the 5CB from the polymerized LC droplets. Right bottom image is a SEM image of the templated microparticle. Images are adapted with permission from ref. 40.

The examples in the previous section of this Perspective Article illustrated select advances involving the interactions of surfactants and LCs, addressing how amphiphilic molecules self-assemble within topological defects and at the aqueous interfaces of LCs. In this section, we move to consider progress in the design of soft matter systems involving polymers and LCs. As noted in the Introduction, a large number of past studies have reported LC-templated polymerizations, with the structure of the resulting polymer networks strongly influenced by LC ordering.[79-81]These studies have been motivated by the potential of LC-templated polymerization to yield both fundamental insights (e.g., visualization of LC orientation[82-84] and defect structures,[30, 41] Figs. 1f and 2g) and technologically relevant advances (e.g., for fabrication of microparticles,[7, 39, 40, 85, 86] nanofiber arrays[87-89], and actuators[90-94] or photonic devices[95-99] based on LC polymer networks and elastomers) into the design of LC-based materials. For example, Mondiot and others,[7, 39, 40] have described how LC microdroplets with distinct internal configurations (e.g., bipolar and radial configurations in Fig. 1g, h) can be used as templates for the synthesis of microparticles with tailored shape and internal pore structure via photopolymerization of reactive mesogens doped into the LC droplets formed from non-reactive mesogens (Fig. 5a). Specifically, as the reactive mesogens aligned parallel to the director of the confined LC, the polymeric network formed within the LC was templated by the internal LC configuration of the droplet (Fig. 5b). Following

subsequent extraction of the non-reactive mesogens, a radial LC droplet (Fig. 1h) was shown to yield a spherical but nanoporous polymeric microparticle, and LC droplets within other configurations resulted in the synthesis of anisometric microparticles including spindle-shaped (Fig. 5b), spherocylindrical, and tear-shaped microparticles (using bipolar, axial, and preradial LC droplet configurations, respectively). While a range of approaches have been reported for synthesis of non-spherical microparticles over the past decade (see references cited within 39 and 40), an advantage of the approach based on LC droplets is the scalable nature of the synthesis.

3.2. Chemical Vapor Deposition into LCs

Despite the long history of polymerization performed in LCs, the fidelity of polymeric nanostructures synthesized by using LC templates is typically limited by changes in LC phase behavior caused by the monomers preloaded into the LC, and the subsequent dynamic evolution of the LC template structure during reaction and consumption of those monomers.[17, 89, 90] This fundamental limitation has i) restricted the types of LCs and monomers that can be used to create LC-templated materials, including the chemical diversity of the resulting polymers, ii) limited the precision with which polymer nanostructures that can be defined using LCs, and iii) limited technological applications of LC-templated polymers due to residual, unreacted monomer (e.g., polymer stabilized LC displays[100, 101]). Recently, an approach was reported that overcomes these broad limitations by demonstrating that polymerization in LCs performed via chemical vapor deposition (called chemical vapor polymerization; CVP) does not significantly change the phase behavior of the LC.[42] The approach was shown to permit synthesis of oriented arrays of end-attached polymeric nanofibers on surfaces with programmable size, shape, and chemical functionality (Fig. 6a). For example, CVP was performed into blue phase LCs that are notoriously difficult to use as templates for polymerization because the blue phase is stable only over a very narrow temperature range.[17] CVP into blue phase LCs yielded a 3-dimensional network of helical nanofibers without perturbation of the phase boundary of the blue phase (Fig. 6b). In addition, the work demonstrated that CVP into LCs is versatile in terms of i) the range of LC phases that can be used as templates (hybrid nematic films led to banana-shaped nanofibers (Fig. 6c); smectic A phases templated nanofibers with broadened tips (Fig. 6d); and cholesteric phases yielded chiral nanofiber assemblies (Fig. 6e)), ii) the ways in which the organization of the phases can be manipulated (e.g., addition of chiral dopants, surface interactions, electric field), iii) the methods

that can be used to deposit the LC template (e.g., spin-coating, inkjet printing, electrified spray), iv) the geometries in which the templates can be used (e.g., wells, films, and droplets), and v) the chemistries of templated nanofibers and their functional properties. Overall, the study demonstrated formation of nanofibers with tunable adhesive, water-repelling, semiconducting, biodegradable, or polycationic properties, including nanofibers that mediates adhesion between two surfaces in a stereo-selective manner (Fig. 6f).

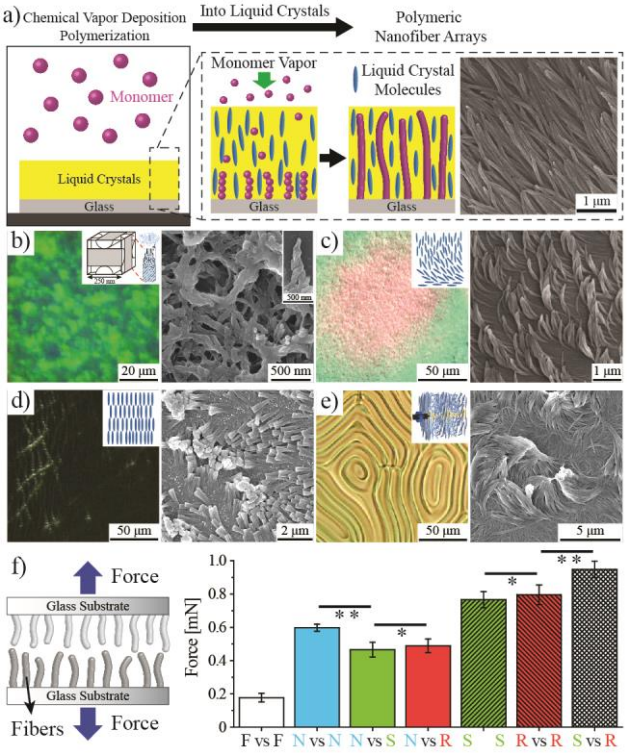

Fig. 6 **(a)** Synthesis of end-attached arrays of polymer nanofibers via chemical vapor deposition polymerization (CVP) into a LC film with homeotropic anchoring and SEM image of the templated nanofibers. **(b-e)** Optical micrographs (crossed polars, left) of LC templates and SEM images (right) of nanofibers templated from films of **(b)** blue phase LC with a cubic lattice spacing of ~250 nm. **(c)** nematic phase with a hybrid anchoring, **(d)** smectic A phase with a homeotropic anchoring, and **(e)** cholesteric LC phase with a left-handed helix. Insets in left images are schematic illustrations of molecular order within the LC templates. **(f)** Adhesion forces measured between pairs of surfaces presenting either flat CVP films (F) or nanofiber arrays templated from nematic (N), left-handed cholesteric (S) or right-handed cholesteric (R) LCs. Images are adapted with permission from ref. 42.

4. LCs and Colloid Science

As described in the Introduction, colloids dispersed in LCs typically experience interparticle interactions that possess complex symmetries.[24-29] The elastic strain of LCs and the associated topological defects induced by colloids play a central role in determining the anisotropic interparticle interactions. Factors that influence the elastic strain and defect formation include colloid, shape and size, as well as surface-induced ordering of LC. Significantly, by using LCs as solvents, it is possible to access colloidal assemblies with precisely defined structures that cannot be prepared in isotropic solvents.[24-29, 53, 54] In this section, we first provide an introduction to colloidal dispersions in LCs and then present two examples, involving hard and soft colloids, that serve to illustrate recent advances in understanding of how colloids can be designed to manipulate interparticle interactions in LCs.

4.1. Hard Colloids in LCs

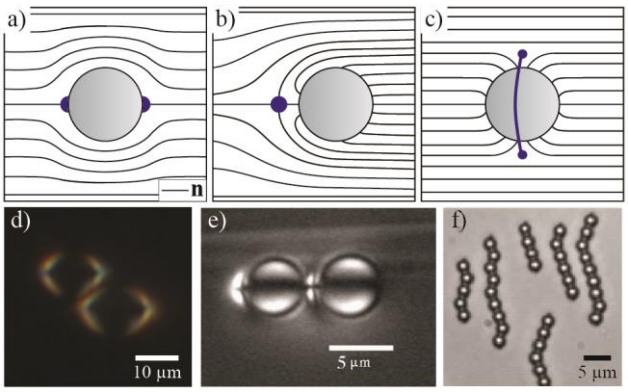

Fig. 7 (a-c) LC director profiles (black lines) near microparticles with **(a)** a tangential anchoring (quadrupolar symmetry), or homeotropic anchoring with **(b)** a hedgehog defect (dipolar symmetry) or **(c)** a Saturn-ring defect (quadrupolar symmetry). Blue dots and line indicate defects. **(d-f)** Optical micrographs of assemblies of microparticles shown in **a-c**, respectively. Images are adapted with permissions from refs. 25, 27, and 104.

When a rigid colloid is dispersed into a nematic host, the orientation of LC around the colloid is determined by a competition between the elastic energy (KR) associated the strain of the LC and the orientation-dependent surface anchoring energy (WR^2), where K is the Frank elastic constant

of the LC, W is the surface anchoring energy density, and R is the radius (size) of the particle. Large colloids, defined as $R > K/W$ (i.e., $WR^2 > KR$), will cause the neighboring LCs to deviate from the far-field orientation ($\mathbf{n}_0$) to satisfy the anchoring condition at the surface of the colloid (e.g., planar and homeotropic anchorings), resulting in LC elastic strain and formation of topological defects.[1, 2] In Fig. 7a-c, we show three representative director profiles (solid lines) and associated defects (blue dots and line) formed around spherical colloids with $R > K/W$.[2, 28] Specifically, the colloid with tangential anchoring generates two point defects (so-called boojums) at its poles and a director profile with quadrupolar symmetry (Fig. 7a).[25, 54, 102-105] However, the particle with homeotropic anchoring can induce a director profile with either dipolar symmetry and a point defect in the bulk LC (hyperbolic hedgehog, Fig. 7b) or quadrupolar symmetry with a disclination loop (Saturn-ring defect, Fig. 7c).[24-27] These dipolar and quadrupolar strains generate elastic interactions between the colloids that have electrostatic analogies, thus providing the basis of simple and predictable designs of programmable colloidal assemblies. For example, microspheres with quadrupolar symmetry (Fig. 7a, c) form chains inclined at an angle from $\mathbf{n}_0$ (Fig. 7d ,f),[25, 54, 102-105] while microspheres with a hyperbolic hedgehog (Fig. 7b) form linear chains along $\mathbf{n}_0$ (Fig. 7e).[24-27] In addition, with the assistance of optical tweezers, past studies have reported that colloids in LCs can be assembled into stable 2D or 3D arrays with well-defined spatial arrangements.[27, 106-109] The assemblies formed by microspheres with Saturn-ring defects are particularly interesting because the defects fuse into complex knots and links of disclination, providing a rich palette of templates for molecular self-assembly as described in previous sections of this Perspective Article.[110-112]

Whereas early studies of colloidal dispersions in LCs focused on spherical particles,[24-29, 53, 54, 102-112], recent advances in colloidal fabrication techniques have enabled exploration of the behaviors of particles with non-spherical geometries.[113] In these studies, the shapes of particles have been shown to play a key role in determining the distortion of the director and associated formation of defects, permitting identification of new principles for controlling colloidal assembly. For example, Smalyukh *et al.*[43-45] investigated LC dispersions of polygonal prisms (e.g., triangle, square, pentagon, and hexagon) and demonstrated their interactions to depend on the number of particle sides and surface anchoring conditions (Fig. 8). Specifically, with tangential anchoring, the colloidal prisms with odd numbers of sides (e.g., triangles (Fig. 8a), pentagons (Fig. 8c)) generated director configurations with dipolar symmetry, leading to dipolar interactions between

the particles (Fig. 8d, e). In contrast, particles having even number of sides (e.g., square (Fig. 8b)) yielded quadrupolar director distortions and thus quadrupolar inter-particular interactions (Fig. 8f).[43] Polygonal prisms with homeotropic anchoring, however, formed disclination loops at the prism edges, leading to dipolar director configurations (Fig. 8g-j) independent of the number of sides.[44, 45] In particular, the orientations of the dipole moments were shown to change upon repining of the disclinations at different edges via local-melting of the LC using laser tweezers (Fig. 8k, l)[45] or reshaping of the prisms into truncated pyramids (Fig. 8m, n).[44] Further work by the same group found that elastic interactions between chiral colloids depend on their handedness.[46, 114]

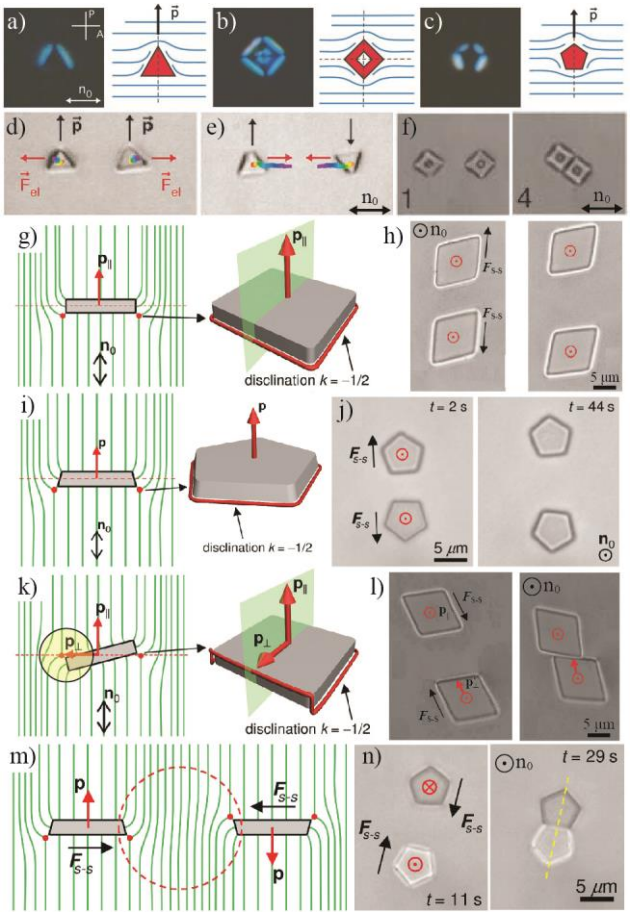

Fig. 8 (a-c) Optical micrographs (left) and director profiles (right) around **(a)** triangle-, **(b)** square-, and **(c)** pentagon-shaped prism particles with tangential anchoring. $\mathbf{n}_0$ and $\vec{p}$ indicate the far-field director and the dipole moment, respectively. **(d, e)** Dipolar elastic interactions (F_{el}, red arrows) of triangular colloids of **a** with **(d)** parallel and **(e)** antiparallel dipole moments. **(f)** Sequential

micrographs showing the quadrupolar elastic interactions of square particles of **b**. The lateral edge lengths of triangles, squares, and pentagons are 3.0 μm, 4.5 μm, and 1.5 μm, respectively. **(g-j)** Director profiles around **(g)** square and **(i)** pentagon prism particles with homeotropic anchoring, and **(h, j)** micrographs for repulsive dipolar interactions ($F_{s\text{-}s}$) between corresponding particles. **(k)** Director profiles around the square particle of **g** following re-pinning of disclinations via the local melting (yellow circle) of LC using an optical tweezer. **(l)** Sequential micrographs showing the attractive elastic interaction between the square particles of **g** (top particle) and **k** (bottom particle). **(m)** Director profile and **(n)** sequential micrographs showing the attractive elastic interaction between antiparallel dipoles of truncated pyramids of **i**. Images are adapted with permissions from refs.43, 44, and 45.

4.2. Soft Colloids in LCs

In contrast to hard colloids described in the previous section, many colloids found in biological systems, such as bacteria and vesicles,[115-119] are soft and readily deformed by external forces (e.g., hydrodynamic forces). Whereas the physical characteristics of soft biological colloids have been extensively studied within isotropic liquids, only recently have soft colloids in LCs been explored.[47, 48] These studies have been enabled by the realization that self-assembled biological structures can be dispersed in lyotropic chromonic LCs (LCLCs) formed by aqueous solutions of disodium cromoglycate (DSCG, Fig. 9a).[58] When dissolved in water, DSCG molecules stack into nanofibrils (green bars in Fig. 9b) and form nematic phases that are influenced by temperature and concentration of DSCG. Recent studies,[47, 48] as detailed below, have used nematic phases of DSCG to explore how strain is shared when soft colloids are dispersed in LCs. These studies reveal that the anisotropic elasticity of LCs enables bending and stretching of soft colloidal species, tuning shape and functional properties.[47, 48]

As discussed below in Section 4.4, living bacteria can be dispersed in LCLCs formed from DSCG without obvious sign of toxicity.[50, 51, 120-123] Of relevance to the study of soft colloids, Mushenheim *et al.*[120] showed that bacterial cell bodies can be sufficiently soft to be deformed by elastic stresses of the LC. Specifically, when long swarm cells of *Proteus mirabilis* were confined in a hybrid LC film (in the limit $L_{\text{bacteria}} > d_{\text{film}}$ where L_{bacteria} is the length of bacterial cell body and d_{film} is the thickness of the LC film), the swarm cells were strained into a bent configuration, thus following the LC director profile within the hybrid film (Fig. 9c, d). The study demonstrated that

the energetic cost of bending a swarm cell is comparable in magnitude to the LC elastic energy, yielding a strong coupling between bacterial shape and elastic strain of LCs. Moreover, the results hint at novel ways to measure mechanical properties of bacterial cells by modulating elastic strains of LCs, which are dependent on thickness of hybrid LC films, temperature, and concentration of DSCG.

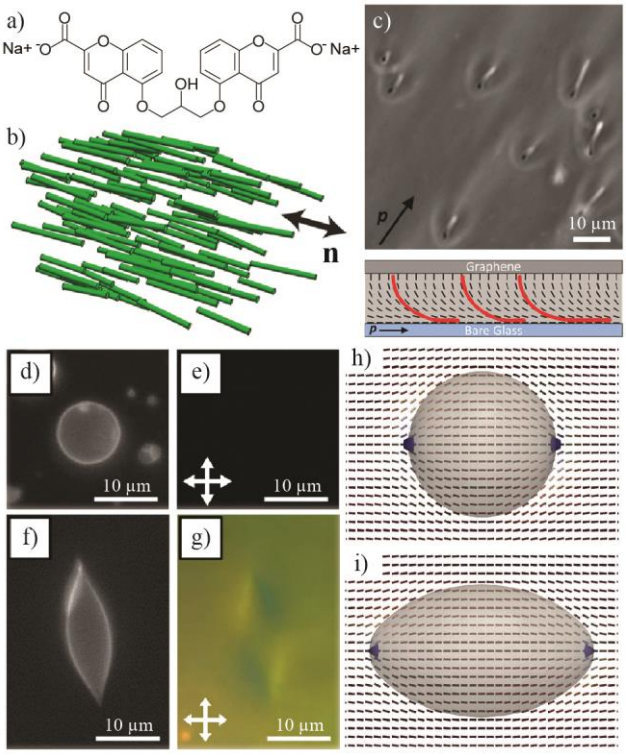

Fig. 9 **(a)** Molecular structure of DSCG. **(b)** Schematic illustration of the long-range orientational order formed by aggregates (green bars) of DSCG. **(c)** Top: phase contrast micrograph of *P. mirabilis* swarm cells confined in a hybrid LC film. Bottom: schematic illustration of the director profile (black dashed line) in the hybrid LC film and the corresponding bent configuration of the swarm cells (red solid line). The direction of the bend and splay distortions within the film is indicated by ***p***. **(d, f)** Fluorescence and **(e, g)** optical micrographs (crossed polars) of giant unilamellar vesicles (GUVs) dispersed in aqueous solution of DSCG at **(d, e)** isotropic and **(f, g)** nematic phases. **(h, i)** Simulated morphology of GUVs in a nematic field with degenerate planar anchoring and their defect structures **(h)** before and **(i)** after deformation. Images are adapted with permissions from refs. 47, 48, and 120.

While the example above describes the bending of bacterial cell bodies by the elastic stress of a LC, the influence of LC phase transitions on dynamic shape transformations of synthetic soft colloids have also been studied using nematic DSCG phases.[47, 48] Specifically, micrometer-sized giant unilamellar vesicles (GUVs) composed of a phospholipid bilayer were shown to adopt spherical shapes in isotropic phases of DSCG in which they were formed (Fig. 9d, e). Upon thermally quenching the aqueous DSCG to form a nematic phase, however, the GUVs were observed to deform into anisotropic shapes, elongating along the far-field director of the LC (Fig. 9f, g). The study revealed that a competition between elastic stresses associated with strained LC and an interfacial energy between the GUV and nematic DSCG controlled the shapes of the GUVs.[47] Simulations of vesicles in LCs have confirmed that nematic elasticity can elongate GUVs in the direction parallel to the local director (Fig. 9h, i).[48] Interestingly, as the GUVs elongate, two boojum defects initially present on the exterior surface of the vesicle are predicted to move into the vesicle interior (blue points in Fig. 9i), a prediction that has not yet been validated by experiments.

4.3. Active Synthetic Colloids in LCs

The studies described above in Section 4.2 address the behaviors of microparticles (including small molecules and colloids) at or close to equilibrium. Inspired by the diversity of dissipative structures and their complex functions found in biological systems, active colloidal systems in LCs have also been explored in recently reported studies.[124, 125] In this context, we note that an important unresolved challenge related to active transport of colloids is lack of control over direction of transport. Specifically, many active colloid systems exhibit rotational Brownian motion, resulting in diffusive-like trajectories at long times.[126, 127] The use of LCs as continuous phases for studies of active colloids has the advantage of offering a fresh set of approaches to control the direction of active transport. Anisotropic viscous drag imposed by LCs on colloidal inclusions, for example, can bias the transport of colloids in both thermotropic and lyotropic LCs.[125, 128-132] However, the effect is modest in magnitude and dominated by other mechanisms identified in recent studies of LCs. For example, a study of silica/Pt Janus microparticles (JPs) adsorbed onto aqueous−LC interfaces reported their active motion, which is driven by platinum metal-catalyzed decomposition of hydrogen peroxide, to be dependent on elastic strain of the LC around JPs.[49] Specifically, the Pt and silica surfaces of the JP create homeotropic and tangential

anchoring of LCs, respectively, leading to preferred orientations of JPs at aqueous-LC interfaces. Four possible orientations of JPs were observed at the aqueous−LC interfaces (Fig. 10) with one of the four orientations (Fig. 10d) shown to correspond to a minimization in the free energies associated with LC elastic deformation and topological defect formation around the JP.[49] The resulting strong orientational coupling between the colloid and LC leads to unidirectional propulsion of the colloid along the LC director.

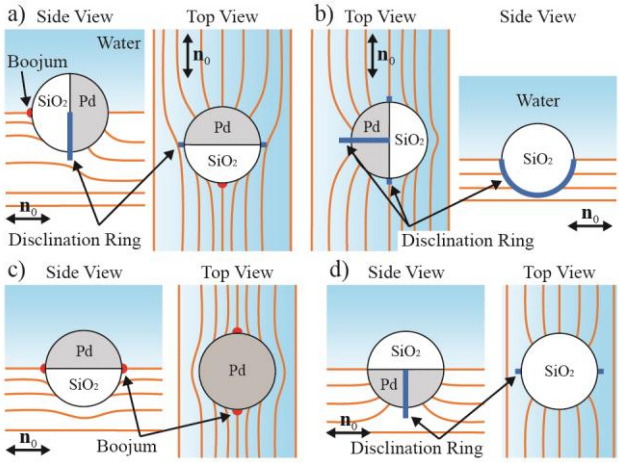

Fig. 10 (a-d) Schematic illustrations depicting topological defects and director profiles (orange lines) around four different Janus particle orientations at the aqueous−LC interface. Red dots are point defects (boojum) and blue lines are disclination lines. Images are adapted with permission from ref. 49.

4.4. Motile Bacteria in LCs

Another advance involving active particles and LCs revolves around motile bacteria in LCLCs (Fig. 9c). These studies revealed a complex coupling between activity-triggered flow and long-range orientational order of the LC.[50, 51, 120-123] A range of observations have been reported, including i) nonlinear bacterial trajectories guided by spatially patterned director profiles, ii) local melting of LC caused by bacteria-generated shear flow, and iii) an activity-triggered transition from a non-flowing uniform state into a flowing one-dimensional periodic pattern and its evolution into a turbulent array of topological defects. In this section, we focus on questions regarding 1) the interplay of LC elasticity and dynamic self-assembly, and 2) competition between LC elasticity and wall-induced hydrodynamic torques acting on bacteria close to surfaces.

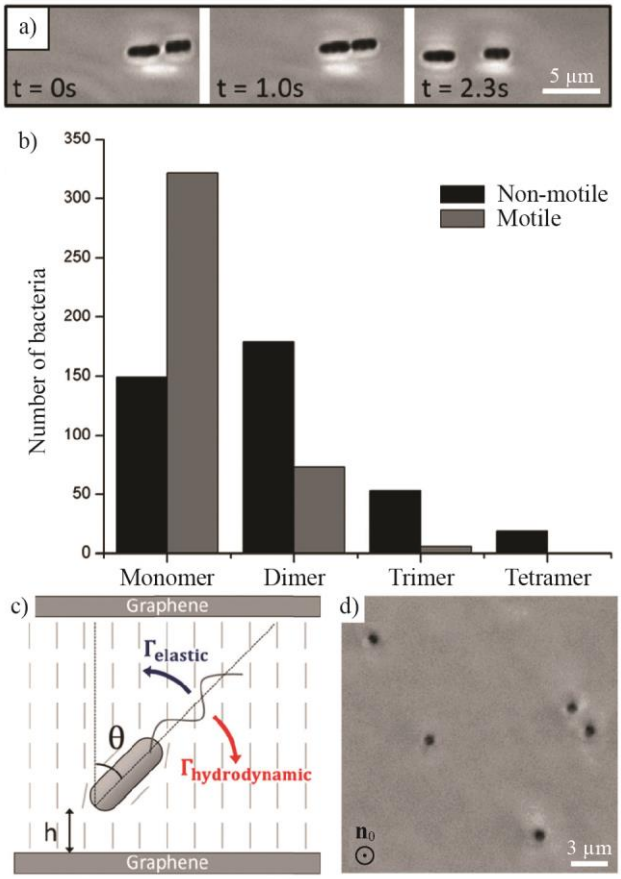

Fig. 11 **(a)** Sequential micrographs showing both the dynamic association and dissociation of two motile bacteria in nematic DSCG solution at 25 °C. **(b)** Populations of multi-cellular complexes formed in nematic DSCG solution by non-motile (black) and motile (gray) bacteria. The total number of cells in both populations is 400. **(c)** Schematic illustration (side view) of the elastic ($\Gamma_{elastic}$) and hydrodynamic ($\Gamma_{hydrodynamic}$) torques acting on a motile bacterium in a homeotropic LC film. Dashed grey lines indicate the orientation of LCs. **(d)** Phase contrast micrograph (top view) depicting the orientation of cells within the homeotropic LC film. Images are adapted with permissions from refs. 51 and 120.

As discussed in the section above on colloidal assembly, extensive work has been carried out previously to characterize the behavior of micrometer-sized synthetic particles (e.g., polystyrene or silica) dispersed within LCs.[24-29, 43-46, 102-112] Typically, LC-mediated elastic interactions are strong, ~100 K_BT, leading to kinetically trapped states that can only be overcome via use of external fields (e.g., optical tweezers).[2, 28] A recent study addresses the question of

whether active colloids provide a way of overcoming kinetically trapped states in LCs, thus creating dynamic assemblies of micrometer-sized particles in LCs.[51] The study found that flagella-derived forces are sufficiently large to overcome elastic attractions between cells (Fig. 11a). Specifically, by comparing populations of dimers, trimers, tetrameters of motile and non-motile cells, motile monomers were measured to be twice as likely as non-motile monomers, whereas the population of non-motile dimers was enriched relative to motile dimers (Fig. 11b). Similar trends were observed for populations of motile and non-motile trimers and tetramers (Fig. 11b). To understand these observations, LC-mediated elastic forces acting between bacteria were estimated from the surface anchoring energy W and quadrupolar distortions of the director as $F_{\text{elastic}} \propto C(W^2R^2/K)(2R/d)^6$ (where d is the distance between the surfaces of the two rod-shaped bacteria, and C is a coefficient of order one) to be $F_{\text{elastic}} \sim 10$ pN at $d = 0.3$ μm. The study concluded that F_{elastic} was comparable to the propulsive forces generated by flagellar motion, supporting the experimental observation that active systems can provide access to reversibly assembling microparticles formed in LCs.

A second set of observations that we highlight here involves motile bacteria and their orientations near surfaces. It is well known that bacteria that propel themselves via a "pushing" mechanism are guided, via hydrodynamic interactions, to swim in parallel to surfaces. A recent study explored how the LC orientations couple to the motion of motile bacteria near interfaces. The study focused on the case where the LC orientation was homeotropic (Fig. 11c).[120, 123] In this scenario, the elastic torque (Γ_{elastic}) promoted alignment of the long-axis of the bacterial cell in a direction normal to the surface. The hydrodynamic torque ($\Gamma_{\text{hydrodynamic}}$) forces, as described above, however, promoted an orientation of the cell and motion that was parallel to the surface. In experiments, it was observed that motile bacteria align normal to the surface (Fig. 11d). Using a simple scaling argument, the study revealed that the elastic torque was larger than the hydrodynamic torque by a factor of ~6 ($\Gamma_{\text{elastic}} / \Gamma_{\text{hydrodynamic}} \sim 6$), thus supporting the experimental observation that the elastic LC interactions dominate hydrodynamic interactions of the bacteria with the surfaces. A range of additional observations have been reported at interfaces between isotropic and nematic DSCG phases (of so-called tactoids)[122, 133, 134] and at surfaces with patterned LC orientations.[135-137] The essential observation is that the elastic stresses of the LC force the bacteria to follow the LC director.

4.5. Self-Reporting and Self-Regulating LC Materials and their Interactions with Motile Cells

In the last section of this Perspective Article, we briefly describe a recent additional study that has reported the design of responsive soft LC-based materials based on chemomechanical interactions of living cells and LCs.[138] In particular, the work provides the first example of a material with the capability to provide a self-regulated release of chemoactive agents in response to mechanical stresses generated by motile bacterial cells, as shown in Fig. 12. The approach was based on formation of micrometer-sized aqueous droplets within LCs, and the demonstration that it was possible to trigger the release of the microdroplets ("microcargo") using targeted physical, chemical, and biological events in ways that can be preprogrammed through an interplay of elastic, electrical double-layer, buoyant, and shear forces (e.g., in wells, films, and droplets). Specifically, it was demonstrated that microdroplets with a radius $R > K/W$ are sequestered within bulk LC due to a strong repulsive elastic force (F_E) acting between the microdroplet surface and LC interfaces (e.g., aqueous−LC, air−LC, and solid−LC interfaces).[139, 140] By decorating the microdroplets with the cationic surfactant DTAB, the authors introduced an attractive electrical double layer interactions (F_{EDL}, Fig. 12a) between the droplets and the interface to a bulk aqueous phase (see Figure 12) that was tuned to be slightly weaker than $|F_E|$ by adjusting the concentration of DTAB (C_{DTAB}); the aqueous−LC interface possesses an excess negatively charge. When motile bacteria were introduced into the overlying aqueous phase, interfacial shear stresses generated by the swimming motion of bacteria were observed to cause the LC to reorient from an initial tangential orientation, leading to i) self-reporting of the arrival of bacteria via generation of a macroscopic optical signal (Fig. 12e) and ii) triggering of the release of microdroplets containing antibacterial agent (Fig. 12c) via changes in the orientation-dependent competing forces, F_E and F_{EDL} (Fig. 12a); F_{EDL} increases while F_E decreases as the orientation of the LC moves away from tangential anchoring. Importantly, the response of the LC material was self-regulating as cell death resulted in cessation of the trigger (mechanical shear stresses of the moving bacteria) that ejected the microdroplets (Fig. 12d): cell death was also reported by the optical response of the LC material (Fig. 12e).

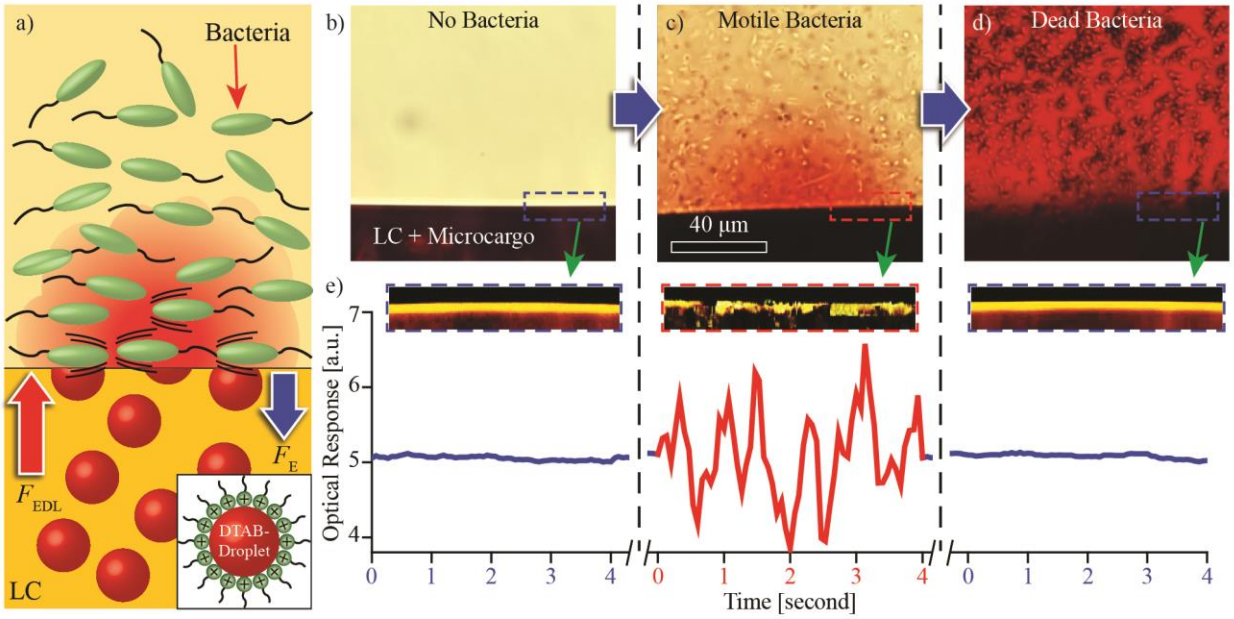

Fig. 12 (a) Illustration (side view) and **(b-d)** sequential micrographs (side view) showing interfacial shear stresses generated by motile bacteria (10^7–10^8 *E. coli* cells/ml) triggering the self-regulated release of microdroplets containing anti-bacterial agent (C_{DTAB} = 2 mM and silver salts) and red tracer, **(b)** before the arrival of bacteria, **(c)** immediately after the arrival of motile bacteria and **(d)** two hours after the arrival of bacteria and following cell death. **(e)** Optical responses and side views of the LC interface corresponding to **b**–**d**. Images are adapted with permission from ref. 138.

5. Conclusions

This Perspective Article describes select advances involving LC-based soft matter systems that have emerged from research performed at the interface of LC, surfactant, polymer and colloid sciences. We end this article by identifying some key open issues and opportunities that are motivated by the examples presented in this review. These issues point to areas of future research that have the potential to provide both fundamental and practical advances in the design of LC-based soft matter systems.

1) Selective self-assembly of amphiphiles within defects. In Section 2.1, we described how polymerized lipid assemblies can be templated from the core of a point defect of strength N = +1 (as characterized optically). The study revealed the nanoscopic structure of the defect to be a toroid (disclination loop of strength m = +1/2; Fig. 2a-g).[30] Interestingly, however, lipid did not

assemble under the same conditions (concentration of lipid) within the cores of defects having strength $N = -1$. This observation highlights the need for additional studies to understand how the strength of a defect impacts molecular self-assembly, and also to understand how the molecular architectures of amphiphiles (and, for example, their spontaneous curvature) impact their self-assembly in topological defects of LCs. Both super-resolution optical microscopy and fluorescence confocal polarizing microscopy appear promising techniques for characterization of self-assembly of amphiphiles in topological defects. The development of a more complete understanding of molecular self-assembly in defects has the potential to provide bottom-up approaches that permit nanoscale wiring of devices and, more generally, fabrication of nanoscopic conduits for directing transport processes (e.g., in nanoreactors or membranes).

2) Influence of molecular structure of amphiphiles on LCs ordering at aqueous interfaces. Several recent studies presented in Section 2.2 have described how the molecular structures of amphiphiles adsorbed at aqueous−LC interfaces influence the ordering of LCs. While these past studies did not observe measurable effects of amphiphile head-group type on interfacial ordering of LCs, independent studies have reported that simple salts can impact the orientations of LCs at aqueous interfaces in a manner that depends on specific salt type.[141, 142] This latter set of observations leads us to predict that future studies will likely find evidence that surfactant head group type does, in fact, influence LC anchoring. The current incomplete understanding of the mechanisms by which amphiphiles influence the anchoring of LCs at aqueous interfaces (as discussed in Section 2.2) also indicates that additional structure-properties studies will likely yield improved designs of amphiphiles for use in LC-based schemes for amplification of biomolecular interactions (e.g., reporting enzymatic processes, protein-ligand binding events).

3) Chemical vapor polymerization into LCs. CVP into LCs appears to be a promising and potentially versatile approach for synthesizing arrays of end-attached, LC-templated polymeric nanofibers on surfaces (Section 3.2). However, many fundamental aspects of CVP in LCs remain to be understood. Specifically, additional studies are needed to provide insight into chemical intermediates formed during LC-templated CVP, knowledge that will provide guidance regarding the chemical diversity of monomers that are compatible with this process. Additionally, studies are needed to understand the properties of the polymeric nanostructures formed by the process, including adhesive interactions between surfaces decorated with arrays of LC-templated CVP nanofibers (Fig. 6f). This knowledge will permit the full capabilities of this scalable advanced

manufacturing process to be realized. For example, we envisage that polymer networks formed by CVP in LCs will enable tailoring of the electrooptical properties of LC films without the detrimental effects of residual monomer that have hindered past efforts to use polymer networks in this way. Other potential applications of LC-templated CVP nanofibers include the preparation of surfaces that possess biomimetic 3D nanoscale topography for cell culture.

4) Hard colloids in LCs. Past studies have established that colloid shape and LC surface anchoring play a key role in defining interactions between colloidal particles in LCs (Section 4.1). Independent investigations have revealed that surface anchoring of LCs can be switched by irradiating immobilized photo-sensitive molecules (e.g., azobenzene units).[143-146] This approach to dynamic manipulation of LC anchoring has the potential to enable future directions of investigation leading to active control of colloidal assembly processes, a prediction that is supported by some recent studies.[147, 148] In addition, an untapped opportunity exists to build on a recent study of LC-in-LC emulsions (thermotropic LC droplets in water-based LCs) in which the orientational ordering of two LC phases was shown to be coupled via van der Waals interactions.[149, 150]

5) Soft colloids in LCs. Studies of giant unilamellar vesicles (GUVs) formed from phospholipids have demonstrated that the membranes of GUVs can be strained by chromonic LCs to the point where transient pores span the GUV membrane (Section 4.2). The opening of the pores permits an efflux of LC through the GUV membrane, resulting in a decrease in the internal volume of each GUV. Interestingly, subsequent transfer of strained GUVs from nematic to isotropic phases results in reformation of spherical GUVs.[47] The mechanisms by which spherical GUVs are recovered upon removal of the elastic stresses are not yet understood, given the strain-induced efflux of internal volume when GUVs are dispersed in the nematic phase. Overall, the studies described in Section 4.2 reveal a complex sharing of strain between soft colloids and LCs, creating fresh opportunity for the design of responsive and reconfigurable materials. We note also that the simulations of GUVs in LCs[48] have not yet incorporated the effects of strain on poration of membranes. In the long term, we predict that the strain-response of soft colloids in LCs will enable development of new methods to characterize the mechanical properties of biological species such as mammalian cells. Changes in the mechanical properties of mammalian cells are often associated with diseased states of the cells, and thus LCs may offer the basis of new diagnostic tools for cell biology and medicine.

6) Motile bacteria in LCs. Sections 4.2 and 4.4 summarize recent studies in which LCs have been used to direct the motion of bacteria, including guiding of motile cells along prescribed non-linear trajectories defined by the LC director (Section 4.2 and 4.4). Examination of the literature reveals several key unresolved issues. First, whereas past studies of *Proteus mirabilis* reveal that elastic strain of the LC around the organisms can generate intercellular forces that result in chaining of cells,[51, 120-122] complementary studies of *Bacillus subtilis* do not report similar elastic interactions.[50, 123] This comparison suggests that bacterial cells likely strain LCs in ways that depend on the specific bacterial cell type. Additionally, an unresolved issue related to studies of bacteria in LCs is that the viscosity of DSCG is too high to permit many bacterial cell types from exhibiting motility. Identification of biocompatible LCs with lower viscosities is an unresolved challenge. Although this latter challenge is large, the design of biocompatible LCs that permit steering of the motion of motile bacterial cells has the potential to yield new tools for detection and characterization of bacteria at the single cell level (thus eliminating the need for cell culture).

7) Interfacial interactions between motile cells and LCs. A recent study has revealed that interfacial shear stresses generated by the swimming motion of motile bacteria at aqueous−LC interfaces can change the orientation of the LC and thus trigger the release of microdroplets (microcargo) that are initially trapped within the LC (Section 4.5). A detailed understanding of the dynamic coupling between bacterial motion and LC orientation at aqueous−LC interfaces, however, is yet to be established (e.g., the role of amphiphilic adsorbates on this coupling; type of swimming motion of organism). This understanding will enable rational design of additional examples of self-reporting and self-regulating LC materials. Such materials offer capabilities that go beyond those typically found in existing biomaterials. For example, they can be designed to release the minimum amount of active agent required to achieve a desired antibacterial effect. This minimizes the release of active agents into the environment, reduces off-target toxicity, and maximizes useful lifetime of the material.

Conflicts of Interest

There are no conflicts to declare.

Acknowledgements

This Perspective Article reviews research that was supported by the Army Research Office (W911NF-15-1-0568 and W911NF-19-1-0071) and the Department of Energy, Basic Energy Sciences, Division of Materials Research, Biomaterials Program under Grant No. DE-SC0019762. Additional support was provided by the National Science Foundation via CBET-1803409 and CBET-1852379.

References

1. P. G. de Gennes and J. Prost, *The Physics of Liquid Crystals*, Clarendon Press, Oxford, 1993.
2. M. Kleman and O. D. Lavrentovich, *Soft Matter Physics: An Introduction*, Springer, New York, 2003.
3. D. Demus, J. Goodby, G. W. Gray, H.-W. Spiess and V. Vill, *Handbook of Liquid Crystals*, Wiley-VCH Verlag GmbH, New York, 1998.
4. D.-K. Yang and S.-T. Wu, *Fundamentals of Liquid Crystal Devices*, John Wiley & Sons, Ltd., Chichester, 2006.
5. A. K. Bhowmik, Z. Li and P. J. Bos, *Mobile Displays : Technology and Applications*, John Wiley & Sons, Ltd, Chichester, 2008.
6. E. Bukusoglu, M. B. Pantoja, P. C. Mushenheim, X. Wang and N. L. Abbott, *Annu. Rev. Chem. Biomol. Eng.*, 2016, **7**, 163-196.
7. D. S. Miller, X. Wang and N. L. Abbott, *Chem. Mat.*, 2014, **26**, 496-506.
8. R. J. Carlton, J. T. Hunter, D. S. Miller, R. Abbasi, P. C. Mushenheim, L. N. Tan and N. L. Abbott, *Liq. Cryst. Rev.*, 2013, **1**, 29-51.
9. A. M. Lowe and N. L. Abbott, *Chem. Mat.*, 2012, **24**, 746-758.
10. P. Popov, E. K. Mann and A. Jakli, *J. Mat. Chem. B*, 2017, **5**, 5061-5078.
11. P. Popov, E. K. Mann and A. Jakli, *Phys Rev Appl*, 2014, **1**, 034003.
12. P. S. Noonan, P. Mohan, A. P. Goodwin and D. K. Schwartz, *Adv. Funct. Mater.*, 2014, **24**, 3206-3212.
13. Y. Liu, D. M. Cheng, I. H. Lin, N. L. Abbott and H. R. Jiang, *Lab Chip*, 2012, **12**, 3746-3753.
14. D. Hartono, W. J. Qin, K. L. Yang and L. Y. L. Yung, *Biomaterials*, 2009, **30**, 843-849.
15. D. Hartono, S. L. Lai, K. L. Yang and L. Y. L. Yung, *Biosens Bioelectron*, 2009, **24**, 2289-2293.
16. J. Xiang and O. D. Lavrentovich, *Appl Phys Lett*, 2013, **103**, 051112.
17. H. Kikuchi, M. Yokota, Y. Hisakado, H. Yang and T. Kajiyama, *Nat Mater*, 2002, **1**, 64-68.
18. H. Y. Chen, C. K. Wu, F. C. Chen and C. S. Chen, *Liq Cryst*, 2016, **43**, 1351-1358.
19. F. Castles, F. V. Day, S. M. Morris, D. H. Ko, D. J. Gardiner, M. M. Qasim, S. Nosheen, P. J. W. Hands, S. S. Choi, R. H. Friend and H. J. Coles, *Nat Mater*, 2012, **11**, 599-603.
20. I. Gvozdovskyy, *Liq Cryst*, 2016, **43**, 1813-1830.
21. H. Yoshida, Y. Tanaka, K. Kawamoto, H. Kubo, T. Tsuda, A. Fujii, S. Kuwabata, H. Kikuchi and M. Ozaki, *Appl Phys Express*, 2009, **2**, 121501.
22. E. Karatairi, B. Rozic, Z. Kutnjak, V. Tzitzios, G. Nounesis, G. Cordoyiannis, J. Thoen, C. Glorieux and S. Kralj, *Phys. Rev. E*, 2010, **81**, 041703.
23. T. A. Wood, J. S. Lintuvuori, A. B. Schofield, D. Marenduzzo and W. C. K. Poon, *Science*, 2011, **334**, 79-83.
24. P. Poulin, H. Stark, T. C. Lubensky and D. A. Weitz, *Science*, 1997, **275**, 1770-1773.
25. P. Poulin and D. A. Weitz, *Phys Rev E*, 1998, **57**, 626-637.
26. J. C. Loudet, P. Barois and P. Poulin, *Nature*, 2000, **407**, 611-613.
27. I. Musevic, M. Skarabot, U. Tkalec, M. Ravnik and S. Zumer, *Science*, 2006, **313**, 954-958.
28. I. Musevic, *Liquid crystal colloids*, Springer Berlin Heidelberg, New York, NY, 2017.

29. I. I. Smalyukh, *Annu. Rev. Condens. Matter Phys.*, 2018, **9**, 207-226.
30. X. Wang, Y.-K. Kim, E. Bukusoglu, B. Zhang, D. S. Miller and N. L. Abbott, *Phys. Rev. Lett.*, 2016, **116**, 147801.
31. Y.-K. Kim, K. R. Raghupathi, J. S. Pendery, P. Khomein, U. Sridhar, J. J. Pablo, S. Thayumanavan and N. L. Abbott, *Langmuir*, 2018, **34**, 10092-10101.
32. H. Ramezani-Dakhel, M. Rahimi, J. Pendery, Y.-K. Kim, S. Thayumanavan, B. Roux, N. L. Abbott and J. J. de Pablo, *Acs Appl Mater Inter*, 2018, **10**, 37618-37624.
33. J. M. Brake, A. D. Mezera and N. L. Abbott, *Langmuir*, 2003, **19**, 6436-6442.
34. N. A. Lockwood, J. J. de Pablo and N. L. Abbott, *Langmuir*, 2005, **21**, 6805-6814.
35. I.-H. Lin, D. S. Miller, P. J. Bertics, C. J. Murphy, J. J. de Pablo and N. L. Abbott, *Science*, 2011, **332**, 1297-1300.
36. D. S. Miller and N. L. Abbott, *Soft Matter*, 2013, **9**, 374-382.
37. L. Adamiak, J. Pendery, J. W. Sun, K. Iwabata, N. C. Gianneschi and N. L. Abbott, *Macromolecules*, 2018, **51**, 1978-1985.
38. Y.-K. Kim, Y. R. Huang, M. Tsuei, X. Wang, N. C. Gianneschi and N. L. Abbott, *Chemphyschem*, 2018, **19**, 2037-2045.
39. F. Mondiot, X. Wang, J. J. de Pablo and N. L. Abbott, *J. Am. Chem. Soc.*, 2013, **135**, 9972-9975.
40. X. Wang, E. Bukusoglu, D. S. Miller, M. A. B. Pantoja, J. Xiang, O. D. Lavrentovich and N. L. Abbott, *Adv. Funct. Mater.*, 2016, **26**, 7343-7351.
41. X. Wang, D. S. Miller, E. Bukusoglu, J. J. de Pablo and N. L. Abbott, *Nat Mater*, 2016, **15**, 106-112.
42. K. C. K. Cheng, M. A. Bedolla-Pantoja, Y.-K. Kim, J. V. Gregory, F. Xie, A. de France, C. Hussal, K. Sun, N. L. Abbott and J. Lahann, *Science*, 2018, **362**, 804-808.
43. C. P. Lapointe, T. G. Mason and Smalyukh, II, *Science*, 2009, **326**, 1083-1086.
44. B. Senyuk, Q. K. Liu, E. Bililign, P. D. Nystrom and I. I. Smalyukh, *Phys Rev E*, 2015, **91**, 040501.
45. B. Senyuk, Q. Liu, P. D. Nystrom and I. I. Smalyukh, *Soft Matter*, 2017, **13**, 7398-7405.
46. Y. Yuan, A. Martinez, B. Senyuk, M. Tasinkevych and I. I. Smalyukh, *Nat Mater*, 2018, **17**, 71-79.
47. P. C. Mushenheim, J. S. Pendery, D. B. Weibel, S. E. Spagnolie and N. L. Abbott, *Proc. Natl. Acad. Sci. U. S. A.*, 2016, **113**, 5564-5569.
48. R. Zhang, Y. Zhou, J. A. Martinez-Gonzalez, J. P. Hernandez-Ortiz, N. L. Abbott and J. J. de Pablo, *Sci. Adv.*, 2016, **2**, e1600978.
49. R. Mangal, K. Nayani, Y.-K. Kim, E. Bukusoglu, U. M. Cordova-Figueroa and N. L. Abbott, *Langmuir*, 2017, **33**, 10917-10926.
50. S. Zhou, A. Sokolov, O. D. Lavrentovich and I. S. Aranson, *Proc. Natl. Acad. Sci. USA*, 2014, **111**, 1265-1270.
51. P. C. Mushenheim, R. R. Trivedi, H. H. Tuson, D. B. Weibel and N. L. Abbott, *Soft Matter*, 2014, **10**, 88-95.
52. O. D. Lavrentovich, P. Psini, C. Zannoni and S. Žumer, *Defects in Liquid Crystals: Computer Simulations, Theory and Experiments*, Springer, Dordrecht, 2001.
53. G. M. Koenig, I.-H. Lin and N. L. Abbott, *Proc. Natl. Acad. Sci. U. S. A.*, 2010, **107**, 3998-4003.
54. I. I. Smalyukh, O. D. Lavrentovich, A. N. Kuzmin, A. V. Kachynski and P. N. Prasad, *Phys Rev Lett*, 2005, **95**, 157801.

55. D. Pires, J. B. Fleury and Y. Galerne, *Phys. Rev. Lett.*, 2007, **98**, 247801.
56. M. Skarabot, M. Ravnik, S. Zumer, U. Tkalec, I. Poberaj, D. Babic and I. Musevic, *Phys Rev E*, 2008, **77**, 061706.
57. J. B. Fleury, D. Pires and Y. Galerne, *Phys Rev Lett*, 2009, **103**, 267801.
58. Y.-K. Kim, S. V. Shiyanovskii and O. D. Lavrentovich, *J. Phys.-Condens. Mat.*, 2013, **25**, 404202.
59. I. F. Lyuksyutov, *Zh. Eksp. Teor. Fiz.*, 1978, **75**, 358-360.
60. N. Schopohl and T. J. Sluckin, *Phys. Rev. Lett.*, 1987, **59**, 2582-2584.
61. E. R. Soule and A. D. Rey, *Soft Matter*, 2012, **8**, 1395-1403.
62. G. E. Volovik and O. D. Lavrentovich, *Zh Eksp Teor Fiz+*, 1983, **85**, 1997-2010.
63. O. D. Lavrentovich, *Liq Cryst*, 1998, **24**, 117-125.
64. M. C. D. Carter, D. S. Miller, J. Jennings, X. Wang, M. K. Mahanthappa, N. L. Abbott and D. M. Lynn, *Langmuir*, 2015, **31**, 12850-12855.
65. J. M. Brake, M. K. Daschner, Y.-Y. Luk and N. L. Abbott, *Science*, 2003, **302**, 2094-2097.
66. M. V. Meli, I. H. Lin and N. L. Abbott, *J Am Chem Soc*, 2008, **130**, 4326-4333.
67. M. Rahimi, H. Ramezani-Dakhel, R. Zhang, A. Ramirez-Hernandez, N. L. Abbott and J. J. de Pablo, *Nat. Commun.*, 2017, **8**, 15064.
68. Y. F. Li, J. J. Y. Suen, E. Prince, E. M. Larin, A. Klinkova, H. Therien-Aubin, S. J. Zhu, B. Yang, A. S. Helmy, O. D. Lavrentovich and E. Kumacheva, *Nat. Commun.*, 2016, **7**, 12520.
69. D. S. Miller, X. G. Wang, J. Buchen, O. D. Lavrentovich and N. L. Abbott, *Anal Chem*, 2013, **85**, 10296-10303.
70. K. Hiltrop and H. Stegemeyer, *Ber Bunsen Phys Chem*, 1978, **82**, 884-889.
71. K. Hiltrop and H. Stegemeyer, *Ber Bunsen Phys Chem*, 1981, **85**, 582-588.
72. U. Kuhnau, A. G. Petrov, G. Klose and H. Schmiedel, *Phys Rev E*, 1999, **59**, 578-585.
73. G. P. Crawford, R. J. OndrisCrawford and J. W. Doane, *Phys Rev E*, 1996, **53**, 3647-3661.
74. V. S. U. Fazio, F. Nannelli and L. Komitov, *Phys Rev E*, 2001, **63**, 061712.
75. A. D. Price and D. K. Schwartz, *J Phys Chem B*, 2007, **111**, 1007-1015.
76. P. D. I. Fletcher, N.-G. Kang and V. N. Paunov, *Chemphyschem*, 2009, **10**, 3046-3053.
77. A. C. McUmber, P. S. Noonan and D. K. Schwartz, *Soft Matter*, 2012, **8**, 4335-4342.
78. P. S. Noonan, R. H. Roberts and D. K. Schwartz, *J Am Chem Soc*, 2013, **135**, 5183-5189.
79. G. P. Crawford, A. Scharkowski, Y. K. Fung, J. W. Doane and S. Zumer, *Phys Rev E*, 1995, **52**, R1273-R1276.
80. Y. K. Fung, D. K. Yang, S. Ying, L. C. Chien, S. Zumer and J. W. Doane, *Liq Cryst*, 1995, **19**, 797-801.
81. I. Dierking, *Adv Mater*, 2000, **12**, 167-181.
82. Y. J. Lee, C. J. Yu, Y.-K. Kim, S. I. Jo and J. H. Kim, *Appl Phys Lett*, 2011, **98**, 033106.
83. Y. Xia, F. Serra, R. D. Kamien, K. J. Stebe and S. Yang, *P Natl Acad Sci USA*, 2015, **112**, 15291-15296.
84. V. P. Panov, S. P. Sreenilayam, Y. P. Panarin, J. K. Vij, C. J. Welch and G. H. Mehl, *Nano Lett.*, 2017, **17**, 7515-7519.
85. M. Schwartz, G. Lenzini, Y. Geng, P. B. Ronne, P. Y. A. Ryan and J. P. F. Lagerwall, *Adv Mater*, 2018, **30**, 1707382.
86. Y. Geng, J. Noh, I. Drevensek-Olenik, R. Rupp, G. Lenzini and J. P. F. Lagerwall, *Sci Rep-Uk*, 2016, **6**, 26840.
87. M. Goh, S. Matsushita and K. Akagi, *Chem Soc Rev*, 2010, **39**, 2466-2476.

88. T. Mori, M. Kyotani and K. Akagi, *Chem Sci*, 2011, **2**, 1389-1395.
89. K. Akagi, *Chem. Rev.*, 2009, **109**, 5354-5401.
90. T. J. White and D. J. Broer, *Nat Mater*, 2015, **14**, 1087-1098.
91. T. Guin, M. J. Settle, B. A. Kowalski, A. D. Auguste, R. V. Beblo, G. W. Reich and T. J. White, *Nat Commun*, 2018, **9**, 2531.
92. A. H. Gelebart, D. J. Mulder, M. Varga, A. Konya, G. Vantomme, E. W. Meijer, R. L. B. Selinger and D. J. Broer, *Nature*, 2017, **546**, 632-636.
93. K. M. Lee, T. J. Bunning and T. J. White, *Adv Mater*, 2012, **24**, 2839-2843.
94. M. T. Brannum, A. M. Steele, M. C. Venetos, L. T. J. Korley, G. E. Wnek and T. J. White, *Adv Opt Mater*, 2019, **7**, 1801683.
95. T. J. White, S. A. Cazzell, A. S. Freer, D. K. Yang, L. Sukhomlinova, L. L. Su, T. Kosa, B. Taheri and T. J. Bunning, *Adv Mater*, 2011, **23**, 1389-1392.
96. T. J. White, M. E. McConney and T. J. Bunning, *J Mater Chem*, 2010, **20**, 9832-9847.
97. T. J. White, R. L. Bricker, L. V. Natarajan, S. V. Serak, N. V. Tabiryan and T. J. Bunning, *Soft Matter*, 2009, **5**, 3623-3628.
98. T. J. White, R. L. Bricker, L. V. Natarajan, N. V. Tabiryan, L. Green, Q. Li and T. J. Bunning, *Adv Funct Mater*, 2009, **19**, 3484-3488.
99. K. M. Lee, V. P. Tondiglia, M. E. McConney, L. V. Natarajan, T. J. Bunning and T. J. White, *Acs Photonics*, 2014, **1**, 1033-1041.
100. Y.-J. Lee, Y.-K. Kim, S. I. Jo, J. S. Gwag, C.-J. Yu and J.-H. Kim, *Opt. Express*, 2009, **17**, 10298-10303.
101. L. Lu, T. Sergan, V. Sergan and P. J. Bos, *Appl Phys Lett*, 2012, **101**, 251912.
102. J. Kotar, M. Vilfan, N. Osterman, D. Babic, M. Copic and I. Poberaj, *Phys Rev Lett*, 2006, **96**, 207801.
103. Y.-K. Kim, B. Senyuk, S. T. Shin, A. Kohlmeier, G. H. Mehl and O. D. Lavrentovich, *Soft Matter*, 2014, **10**, 500-509.
104. Y.-K. Kim, R. Breckon, S. Chakraborty, M. Gao, S. N. Sprunt, J. T. Gleeson, R. J. Twieg, A. Jakli and O. D. Lavrentovich, *Liq Cryst*, 2014, **41**, 1345-1355.
105. Y.-K. Kim, G. Cukrov, F. Vita, E. Scharrer, E. T. Samulski, O. Francescangeli and O. D. Lavrentovich, *Phys. Rev. E*, 2016, **93**, 062701.
106. M. Skarabot, M. Ravnik, S. Zumer, U. Tkalec, I. Poberaj, D. Babic, N. Osterman and I. Musevic, *Phys Rev E*, 2007, **76**, 051406.
107. I. Musevic and M. Skarabot, *Soft Matter*, 2008, **4**, 195-199.
108. M. Skarabot, M. Ravnik, S. Zumer, U. Tkalec, I. Poberaj, D. Babic, N. Osterman and I. Musevic, *Phys Rev E*, 2008, **77**, 031705.
109. A. Nych, U. Ognysta, M. Skarabot, M. Ravnik, S. Zumer and I. Musevic, *Nat Commun*, 2013, **4**, 1489.
110. M. Ravnik, M. Skarabot, S. Zumer, U. Tkalec, I. Poberaj, D. Babic, N. Osterman and I. Musevic, *Phys Rev Lett*, 2007, **99**, 247801.
111. S. Copar and S. Zumer, *Phys Rev Lett*, 2011, **106**, 177801.
112. U. Tkalec, M. Ravnik, S. Copar, S. Zumer and I. Musevic, *Science*, 2011, **333**, 62-65.
113. C. J. Hernandez and T. G. Mason, *J Phys Chem C*, 2007, **111**, 4477-4480.
114. K. Nayani, Y.-K. Kim and N. L. Abbott, *Nat Mater*, 2018, **17**, 14-15.
115. P. A. Giardini, D. A. Fletcher and J. A. Theriot, *P Natl Acad Sci USA*, 2003, **100**, 6493-6498.
116. Y. Sakuma, T. Taniguchi, T. Kawakatsu and M. Imai, *Biophys. J.*, 2013, **105**, 2074-2081.

117. F. C. Keber, E. Loiseau, T. Sanchez, S. J. DeCamp, L. Giomi, M. J. Bowick, M. C. Marchetti, Z. Dogic and A. R. Bausch, *Science*, 2014, **345**, 1135-1139.
118. A. Amir, F. Babaeipour, D. B. McIntosh, D. R. Nelson and S. Jun, *P Natl Acad Sci USA*, 2014, **111**, 5778-5783.
119. H. H. Wensink, J. Dunkel, S. Heidenreich, K. Drescher, R. E. Goldstein, H. Lowen and J. M. Yeomans, *P Natl Acad Sci USA*, 2012, **109**, 14308-14313.
120. P. C. Mushenheim, R. R. Trivedi, S. S. Roy, M. S. Arnold, D. B. Weibel and N. L. Abbott, *Soft Matter*, 2015, **11**, 6821-6831.
121. R. R. Trivedi, R. Maeda, N. L. Abbott, S. E. Spagnolie and D. B. Weibel, *Soft Matter*, 2015, **11**, 8404-8408.
122. P. C. Mushenheim, R. R. Trivedi, D. B. Weibel and N. L. Abbott, *Biophys J*, 2014, **107**, 255-265.
123. S. Zhou, O. Tovkach, D. Golovaty, A. Sokolov, I. S. Aranson and O. D. Lavrentovich, *New J Phys*, 2017, **19**, 055006.
124. Y.-K. Kim, B. Senyuk and O. D. Lavrentovich, *Nat Commun*, 2012, **3**, 1133.
125. O. D. Lavrentovich, *Soft Matter*, 2014, **10**, 1264-1283.
126. W. T. Coffey, Y. P. Kalmykov and J. T. Waldron, *The Langevin Equation: With Applications in Physics, Chemistry and Electrical Engineering*, World Scientific, Singapore, 1996.
127. T. Turiv, I. Lazo, A. Brodin, B. I. Lev, V. Reiffenrath, V. G. Nazarenko and O. D. Lavrentovich, *Science*, 2013, **342**, 1351-1354.
128. H. Stark, D. Ventzki and M. Reichert, *J Phys-Condens Mat*, 2003, **15**, S191-S196.
129. R. W. Ruhwandl and E. M. Terentjev, *Phys Rev E*, 1996, **54**, 5204-5210.
130. J. C. Loudet, P. Hanusse and P. Poulin, *Science*, 2004, **306**, 1525-1525.
131. M. Skarabot and I. Musevic, *Soft Matter*, 2010, **6**, 5476-5481.
132. F. Mondiot, J. C. Loudet, O. Mondain-Monval, P. Snabre, A. Vilquin and A. Wurger, *Phys Rev E*, 2012, **86**, 010401.
133. C. H. Peng and O. D. Lavrentovich, *Soft Matter*, 2015, **11**, 7257-7263.
134. L. Tortora and O. D. Lavrentovich, *Proc. Natl. Acad. Sci. USA.*, 2011, **108**, 5163-5168.
135. C. H. Peng, T. Turiv, Y. B. Guo, Q. H. Wei and O. D. Lavrentovich, *Liq Cryst*, 2018, **45**, 1936-1943.
136. C. H. Peng, Y. B. Guo, T. Turiv, M. Jiang, Q. H. Wei and O. D. Lavrentovich, *Adv Mater*, 2017, **29**, 1606112.
137. C. H. Peng, T. Turiv, Y. B. Guo, Q. H. Wei and O. D. Lavrentovich, *Science*, 2016, **354**, 882-885.
138. Y.-K. Kim, X. Wang, P. Mondkar, E. Bukusoglu and N. L. Abbott, *Nature*, 2018, **557**, 539-544.
139. O. P. Pishnyak, S. Tang, J. R. Kelly, S. V. Shiyanovskii and O. D. Lavrentovich, *Phys. Rev. Lett.*, 2007, **99**, 127802.
140. S. B. Chernyshuk and B. I. Lev, *Phys. Rev. E*, 2011, **84**, 011707.
141. R. J. Carlton, J. K. Gupta, C. L. Swift and N. L. Abbott, *Langmuir*, 2012, **28**, 31-36.
142. J. Zou, T. Bera, A. A. Davis, W. Liang and J. Fang, *J. Phys. Chem. B*, 2011, **115**, 8970-8974.
143. A. Eremin, P. Hirankittiwong, N. Chattham, H. Nadasi, R. Stannarius, J. Limtrakul, O. Haba, K. Yonetake and H. Takezoe, *P Natl Acad Sci USA*, 2015, **112**, 1716-1720.
144. T. Yamamoto, Y. Tabe and H. Yokoyama, *Colloid Surface A*, 2009, **334**, 155-159.

145. T. Ikeda, *J Mater Chem*, 2003, **13**, 2037-2057.
146. K. Ichimura, *Chem. Rev.*, 2000, **100**, 1847-1873.
147. Y. Yuan, G. N. Abuhaimed, Q. K. Liu and I. I. Smalyukh, *Nat. Commun.*, 2018, **9**, 5040.
148. Y. Yuan, Q. K. Liu, B. Senyuk and I. I. Smalyukh, *Nature*, 2019, **570**, 214-218.
149. P. C. Mushenheim and N. L. Abbott, *Soft Matter*, 2014, **10**, 8627-8634.
150. G. Chu, G. Vasilyev, R. Vilensky, M. Boaz, R. Y. Zhang, P. Martin, N. Dahan, S. W. Deng and E. Zussman, *Langmuir*, 2018, **34**, 13263-13273.

Table of Contents

We review advances in soft matter research based on liquid crystals, including recent studies of liquid crystals beyond equilibrium.